JACS
JOURNAL OF THE AMERICAN CHEMICAL SOCIETY
Cite This: J. Am. Chem. Soc. 2018, 140, 13618−13622
Communication
pubs.acs.org/JACS

# Linking Molybdenum−Sulfur Clusters for Electrocatalytic Hydrogen Evolution

Zhe Ji,[†] Christopher Trickett,[†] Xiaokun Pei,[†] and Omar M. Yaghi*[,†,‡]

[†]Department of Chemistry, University of California-Berkeley, Materials Sciences Division, Lawrence Berkeley National Laboratory, and Kavli Energy NanoSciences Institute, Berkeley, California 94720, United States

[‡]UC Berkeley−KACST Joint Center of Excellence for Nanomaterials for Clean Energy Applications, King Abdulaziz City for Science and Technology, Riyadh 11442, Saudi Arabia

Supporting Information

**ABSTRACT:** Controlling the spatial arrangement of molecular catalysts on electrodes is critical to developing an optimal electrocatalyst. Mo−S clusters have shown great promise in catalyzing hydrogen evolution for the generation of carbon-free fuel from water. Here we report a synthetic approach to organize these molecular clusters into ordered dimers, cages, and chains through the use of organic linkers, as solved by single-crystal X-ray diffraction. We find that the linkage through the coordination bond between thiolate and $Mo_3S_7$ leads to (1) a 40-fold enhancement in turnover frequency compared with the unlinked cluster and (2) the periodic arrangement of clusters on the electrode with control over their distance, orientation, and density, thus enabling hydrogen evolution at high catalyst loading. The materials developed here require an overpotential of only 89 mV to achieve a current density of 10 mA $cm^{-2}$, outperforming other Mo−S catalysts (both molecular and solid-state).

Hydrogen production through water splitting is envisioned to satisfy the global demand for clean and sustainable energy.[1,2] To facilitate the implementation of this technology on a wide scale, great efforts have been devoted to identifying efficient and cheap catalysts for the hydrogen evolution reaction (HER).[3−23] $MoS_2$ represents a promising non-noble-metal-based candidate as an alternative to the precious metal platinum,[12,24] which shows one of the best-known hydrogen evolution activities in acidic media. However, only the edges of this layered structure act as active sites, while the basal planes are inert.[12] To maximize the number of catalytically active sites within the material on the electrode surface, bulk $MoS_2$ can be downsized to nanoparticles[6,16] and even discrete clusters.[9,17,18,21−23] In this context, the trinuclear cluster $[Mo^{IV}_3S(S_2)_6]^{2-}$ has been demonstrated as a molecular analogue of the $MoS_2$ edge site, exhibiting state-of-the-art turnover frequencies (TOFs) at submonolayer coverage.[9] Nevertheless, at heavy catalyst loadings required for practical use, the highest current densities delivered by these clusters have not outperformed $MoS_2$-based solids. To translate the high TOF of discrete clusters into a high current density, it is therefore desirable to deposit these molecules on the electrode surface with optimal orientation, distance, and density to enable efficient mass transport, charge transfer, and structural rearrangement of catalysis intermediates.[25,26] Still, controlling the spatial arrangement of molecular clusters on a substrate by design remains an outstanding challenge. In this work, we developed an approach to align Mo−S clusters on electrode surfaces by using organic linkers to connect them through strong chemical bonds into well-defined structures such as dimers, cages, and chains, a group of materials termed metal−organic sulfide (MOS). A member of this series featuring a chain structure displays a 40-fold enhancement in TOF and achieves a current density of 10 mA $cm^{-2}$ at an overpotential of only 89 mV, the latter representing the lowest value among Mo−S compounds. The catalytic efficiency, facile growth on carbon substrates, scalable wet chemistry, and high stability in acidic aqueous electrolytes make these MOS catalysts especially promising in electrocatalysis applications.

Linking metal-containing clusters with organic linkers into extended structures has been widely practiced in the synthesis of metal−organic frameworks (MOFs).[27] An appealing feature of MOFs is the enormous flexibility with which the composition and connectivity of the metal-containing clusters (termed secondary building units, SBUs) can be varied to construct new desirable structures. However, the SBUs employed to date are still mainly limited to metal−oxygen and metal−nitrogen clusters, such as $Zn_4O(CO_2)_6$, $Cu_2(CO_2)_4$, $Zr_6O_4(OH)_4(CO_2)_{12}$, and $Zn(imidazolate)_2$,[28] leaving metal−sulfur clusters largely unexplored.[29,30] In contrast to the regular hard acid and base coordination bonds prevalent in MOF chemistry, sulfido and thiolate linkers provide a unique soft-base linkage, which can lead to properties that cannot be achieved in conventional MOFs. In the context of catalytic hydrogen evolution, the largely polarizable sulfido ligands stabilize the low oxidation state (IV) of molybdenum under reductive conditions, a prerequisite for their use in catalytic hydrogen evolution.[31] In fact, many processes in nature also rely on metal sulfide clusters.[31] Given the diversity and unique properties of metal−sulfur clusters, we sought to explore the reticular chemistry of MOS.

The effort to link metal−sulfur clusters with organic linkers commenced with the $[Mo_3S_{13}]^{2-}$ cluster[32,33] (Scheme 1). This trinuclear cluster features a $Mo_3S_7$ core and three terminal $S_2^{2-}$ ligands, of which the replacement with two bromide anions, resulting in $[Mo_3S_7Br_6]^{2-}$, allows for further ligand sub-

Received: September 10, 2018
Published: October 9, 2018

Downloaded via UNIV OF CALIFORNIA BERKELEY on October 31, 2018 at 19:27:40 (UTC).
See https://pubs.acs.org/sharingguidelines for options on how to legitimately share published articles.


© 2018 American Chemical Society

DOI: 10.1021/jacs.8b09807
J. Am. Chem. Soc. 2018, 140, 13618−13622

**Scheme 1. Synthesis and Linking of $Mo_3S_7$ Clusters by Ligand Substitution**[a]

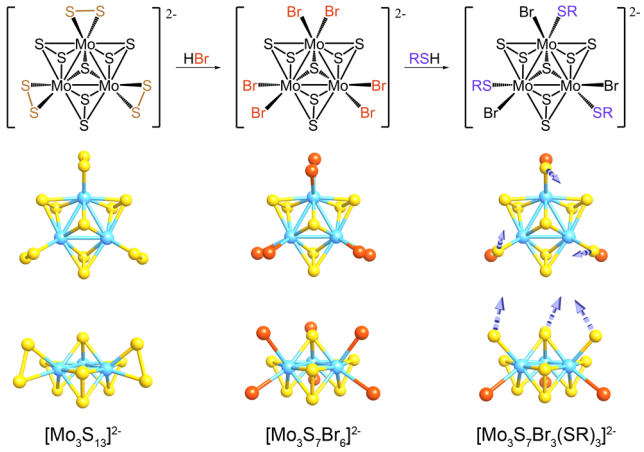


[a]Color code for ball-and-stick models: Mo, blue; Br, orange; S, yellow; R group, purple.

stitution[34,35] into thiolates $[Mo_3S_7Br_3(SR)_3]^{2-}$ (sections S2 and S3 in the Supporting Information). During ligand substitution, the $Mo_3S_7$ core remains intact and the bromide ions are partially replaced on one side of the $Mo_3$ plane, while the bromide ions on the opposite side of each cluster remain bound (Scheme 1).[36] This robust ligand substitution chemistry permits the use of $[Mo_3S_7Br_3(SR)_3]^{2-}$ as a three-connected SBU for reticulation into extended solids.

The linking of the $[Mo_3S_7Br_3(SR)_3]^{2-}$ SBU was attempted by treating $[Mo_3S_7Br_6]^{2-}$ with the ditopic linker 1,3-benzenedithiol (*m*-BDT) (Scheme 2). The addition of an excess of $NEt_4^+$ cation induces the crystallization, leading to a structure identified by single-crystal X-ray diffraction (SXRD) as the dimer $(NEt_4)_4[Mo_3S_7Br_3(m\text{-BDT})_{1.5}]_2$ (MOS-1) (section S4). In the structure, two $Mo_3$ triangles exhibit an eclipsed conformation, which allows the three *m*-BDT linkers to act as bridges, giving rise to a closed capsule shape. To tune the orientation of the clusters with regard to each other, 1,4-benzenedithiol (*p*-BDT) was employed as the linker, affording another dimer, $(NEt_4)_4[Mo_3S_7Br_4(p\text{-BDT})]_2$ (MOS-2), in single-crystalline form (Scheme 2). The structure was elucidated by SXRD and shows an offset between two $Mo_3$ triangles by 60° along their central axis (section S4). This staggered conformation generates a connectivity of only two, leaving each cluster with one bromide ligand available for further linking.

As the staggered conformation can be fixed by using the *p*-BDT linker, the third connection made between cluster dimers led to an extended chain, packing in orange hexagonal-shaped single crystals (Scheme 2 and section S3). SXRD obtained from synchrotron X-ray sources solved the heavy atoms in the structure, suggesting that each cluster is linked by three thiolate linkers (section S4). This connection of three was further confirmed by $^1H$ NMR analysis of digested crystals along with elemental analysis and inductively coupled plasma atomic emission spectroscopy (ICP-AES), giving the formula for MOS-3 as $(NEt_4)_2[Mo_3S_7Br_3(p\text{-BDT})_{1.5}]$ (section S5). To obtain the complete structure, a structure model was built in Materials Studio by fitting benzene rings of the linkers between the clusters (section S5). The modeled chain structure was corroborated by Pawley refinement of the powder X-ray diffraction (PXRD) pattern.

**Scheme 2. $Mo_3S_7$ Clusters Connected by Dithiolate Linkers into Dimers and a Chain**[a]

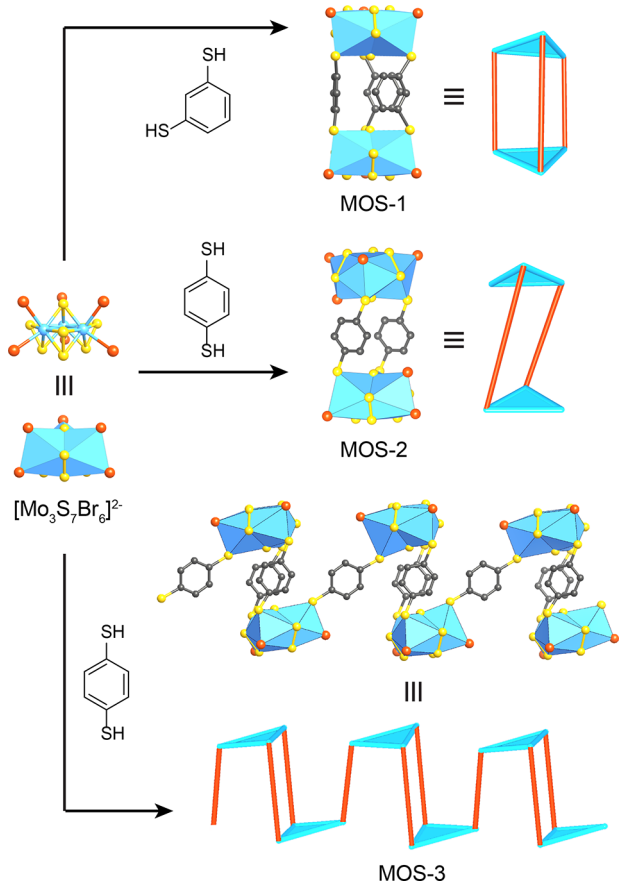


[a]Color code for ball-and-stick models: Mo, blue; Br, orange; S, yellow; R group, purple.

To demonstrate the versatility of the SBU approach of connecting metal−sulfur clusters through rational design, the $Mo_3S_4$ cluster[37,38] was additionally employed as the SBU for the construction of linked structures (section S2). Starting with $[Mo_3S_4(H_2O)_9]^{4+}$, the terminal water ligands can be replaced with the ditopic linker 2,5-dihydroxyterephthalic acid ($H_2DOT$) and pyridine (py), forming the cluster dimer $[Mo_3S_4(py)_3(DOT)_{1.5}]_2^{4-}$ (MOS-4) (Scheme 3 and section S3). The two $Mo_3$ triangles in the dimer are staggered by 15° in the single-crystal structure (section S4). Alternatively, modifying the $Mo_3S_4$ cluster with the tridentate ligand nitrilotriacetic acid ($H_3NTA$) places three carboxylate groups on the periphery, which further connect with $Zn^{2+}$ ions to form a rhombic dodecahedron, $\{[Mo_3S_4(NTA)_3]_8[Zn(H_2O)]_6\}^{28-}$ (MOS-5) (Scheme 3 and section S3). As solved by SXRD, six of the five-coordinated Zn centers occupy the faces of the cage, while eight of the $Mo_3S_4$ clusters sit on the corners, encompassing a pore with a size of 11.4 Å (section S4).

Given the facile synthesis of MOS-1 and MOS-3 and their high stability in aqueous media, we focused on these two members in our investigation of their electrocatalytic HER activity. This was done by using a three-electrode electrochemical cell containing nitrogen-purged 0.5 M $H_2SO_4$ (section S6). Thin layers of MOS-1 and MOS-3 were grown in situ on fluorine-doped tin oxide (FTO) substrates, resulting in a 0.2 nmol $cm^{-2}$ loading (based on $Mo_3$ units) as measured by ICP-AES (section S7). A comparable amount of the



DOI: 10.1021/jacs.8b09807
J. Am. Chem. Soc. 2018, 140, 13618−13622

**Scheme 3. $Mo_3S_4$ Clusters Connected by Linkers into a Dimer and a Cage**[a]

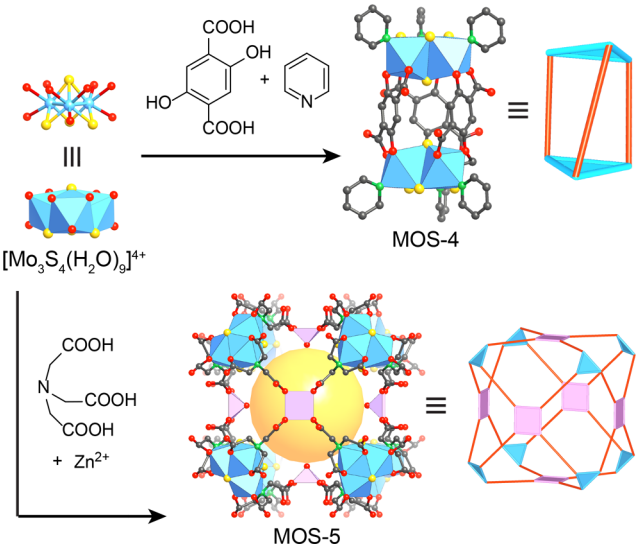


[a]Color code for ball-and-stick models: Mo, blue; Zn, pink; S, yellow; C, gray; N, green; O, red. Color code for topology illustrations: SBUs, blue triangles; linkers, red lines; Zn centers, pink squares; cavity, yellow sphere.

unlinked cluster $[Mo_3S_7Br_6]^{2-}$ was loaded on separate FTO substrates for comparison. While the bare FTO substrate and the $[Mo_3S_7Br_6]^{2-}$ thin layer showed negligible HER activity, both the MOS-1 and MOS-3 samples displayed a sharp exponential increase in the magnitude of the cathodic current density with increasing overpotential, characteristic of catalytic activity (Figure 1a). To compare the HER activities among other catalyst materials, the TOFs of both MOS-1 and MOS-3 at an overpotential of 200 mV were determined to be 1.21 $s^{-1}$ by normalizing the current density by the number of Mo atoms per geometrical area of the electrode surface (section S8). Comparison with the inert unlinked $[Mo_3S_7Br_6]^{2-}$ cluster, with a TOF of 0.03 $s^{-1}$, shows that the organic linking endows MOS materials with high catalytic efficiency, as confirmed by the polarization curve of molybdenum benzenethiolate (section S9). By leveraging the coordination chemistry of the thiolate linker and the $Mo_3S_7$ cluster, MOS materials exhibit enhanced TOFs compared with the state-of-the-art molecular cluster $[Mo_3S_{13}]^{2-}$ under the same conditions (section S9). To shed light on the catalytic mechanism, Tafel plots are shown in Figure 1b. MOS-1 and MOS-3 thin layers exhibit a Tafel slope of 57 mV per decade, suggesting a rate-limiting chemical rearrangement in the Volmer–Heyrovsky HER mechanism (section S10).[6,9,39] This process may involve a Mo–H intermediate, of which the desorption reaction can be facilitated by the thiolate linker.

For practical use, a high current density is necessary and typically achieved by loading large amounts of catalyst onto the electrode. The overpotential required to drive a current density of 10 mA $cm^{-2}$ has been widely adopted as the metric to gauge the efficiency of a catalyst.[7] To prepare a heavy loading, MOS structures were grown onto Super C45, a carbon black (CB) powder, as the conductive matrix by soaking CB in the MOS reaction mixture (section S11). The in situ synthesis led to a uniform coverage of MOS-3 on CB, as evidenced by high-angle

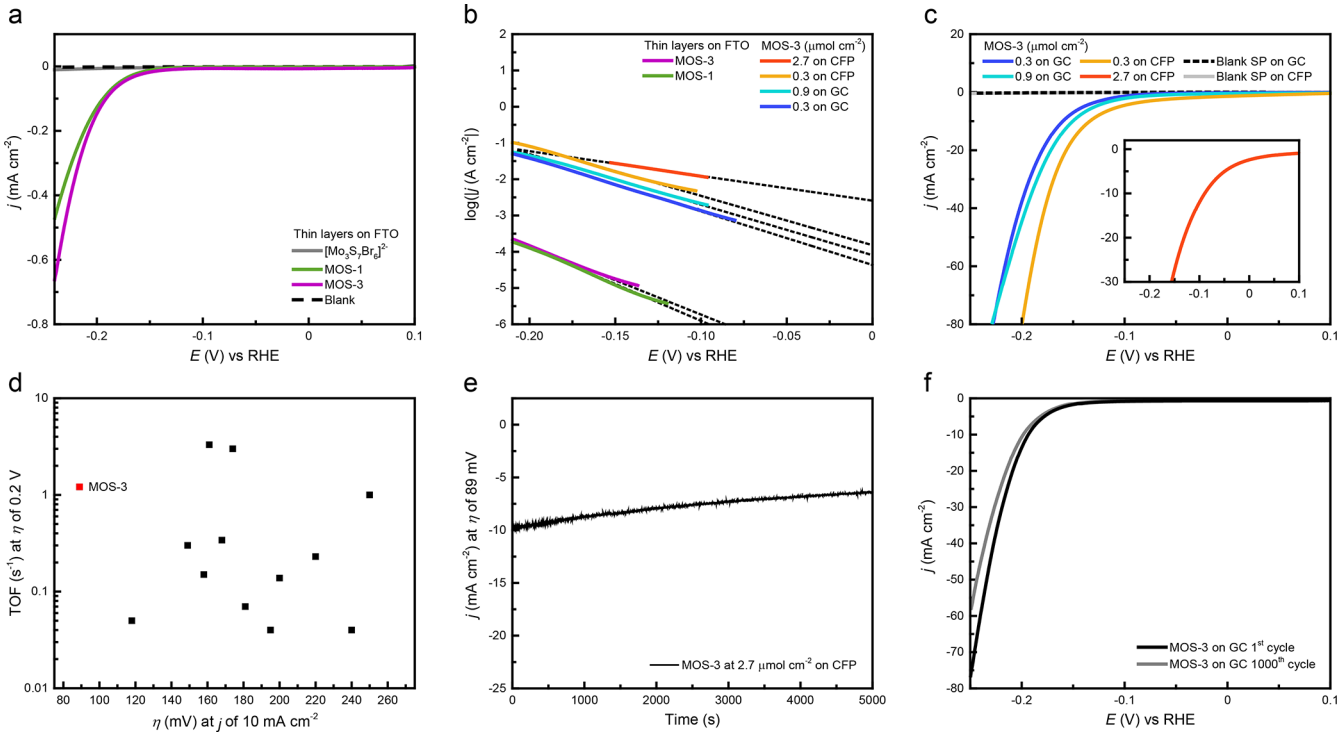


**Figure 1.** HER activities of MOS materials. (a) Polarization curves of thin-layer coverage of $[Mo_3S_7Br_6]^{2-}$, MOS-1, and MOS-3 on FTO. (b) Tafel plots of the polarization curves. (c) Polarization curves of MOS-3 on GC and CFP with various loadings. (d) Comparison between the metrics of Mo–S-based HER catalysts: TOF per Mo at an overpotential ($\eta$) of 0.2 V plotted against the overpotential required for a current density of 10 mA $cm^{-2}$.[5–9,14–20] The values optimized independently for these two parameters are taken (section S12). (e) Chronoamperometry of MOS-3 at $\eta$ = 89 mV with a loading of 2.7 $\mu$mol $cm^{-2}$ on CFP. (f) Initial and postcycling CVs of MOS-3 with a loading of 0.1 $\mu$mol $cm^{-2}$ on GC.



DOI: 10.1021/jacs.8b09807
J. Am. Chem. Soc. 2018, 140, 13618–13622

annular dark-field scanning transmission electron microscopy (HAADF-STEM) and energy-dispersive X-ray spectroscopy (EDXS) mapping. The resulting MOS−CB composites displaying a PXRD pattern consistent with that of MOS-3 were subsequently drop-cast together with Nafion onto a glassy carbon electrode (GC) and carbon fiber paper (CFP). On GC, an increase in catalyst loading delivers an improved current density at low overpotentials, with the Tafel slope unchanged at 70 mV per decade (Figure 1b,c). When CFP was used as the electrode, the current density further increased to 80 mA $cm^{-2}$ at an overpotential of 200 mV, corresponding to a TOF of 0.48 $s^{-1}$ at a loading of 0.3 $\mu$mol $cm^{-2}$. Moreover, by drop-casting a thick layer of MOS-3-CB onto CFP, a current density of 10 mA $cm^{-2}$ was generated at an overpotential of only 89 mV, with an exchange current density of 2.5 mA $cm^{-2}$, setting a new record among Mo−S-based catalysts (Figure 1d and section S12). The catalytic nature of this process was verified by passing 2.8 C of charge during chronoamperometry (Figure 1e). To assess the stability of MOS catalysts, continuous cyclic voltammetry (CV) was performed for thin layers on FTO and heavy loadings on GC and CFP (Figure 1f and section S13). An increase of 10 mV in overpotential was found after 1000 cycles on GC, which is comparable to that of $[Mo_3S_{13}]^{2-}$.[9] The PXRD pattern of the material on GC after 1000 cycles of CV was found to be in good agreement with that of the as-synthesized one (section S11), indicating that our material is durable for long-time usage without loss of crystallinity.

We ascribe this outstanding HER performance to the periodic arrangement of Mo−S clusters on the conductive surface, facilitating the mass transport. As evidenced by Fourier transform infrared (FT-IR) spectroscopy, the bulky $NEt_4^+$ ions between the chains can be readily exchanged to $K^+$ (section S14). The resulting material shows a Brunauer−Emmett−Teller (BET) surface area of 116 $m^2$ $g^{-1}$ calculated from nitrogen adsorption isotherm (section S14). By exposure of a majority of the active sites to the electrolyte, the catalyst loading at the electrode becomes scalable without sacrificing the performance of each active center. Thus, the wet chemistry developed here provides a solid material with well-defined structures at the molecular level that is capable of straightforward synthesis and processing onto the electrode.

## ■ ASSOCIATED CONTENT

### Supporting Information

The Supporting Information is available free of charge on the ACS Publications website at DOI: 10.1021/jacs.8b09807.

Crystallographic data for MOS-1 (CIF)
Crystallographic data for MOS-2 (CIF)
Crystallographic data for MOS-3 (CIF)
Crystallographic data for MOS-4 (CIF)
Crystallographic data for MOS-5 (CIF)
Coordinates for MOS-3 simulation, part A (CIF)
Coordinates for MOS-3 simulation, parts A + B (CIF)
Coordinates for MOS-3 simulation, part B (CIF)
Methods and additional data (PDF)

## ■ AUTHOR INFORMATION


### Corresponding Author

*yaghi@berkeley.edu

### ORCID

Zhe Ji: 0000-0002-8532-333X
Omar M. Yaghi: 0000-0002-5611-3325


### Notes

The authors declare no competing financial interest.

## ■ ACKNOWLEDGMENTS

This work was supported by King Abdulaziz City for Science and Technology (Center of Excellence for Nanomaterials for Clean Energy Applications). The single-crystal X-ray diffraction data were collected at beamlines 11.3.1 and 5.0.2 at the Advanced Light Source, Lawrence Berkeley National Laboratory, which is supported by the Director, Office of Science, Office of Basic Energy Sciences, U.S. Department of Energy, under Contract DE-AC02-05CH11231. The authors thank Dr. Marc Allaire for the synchrotron X-ray diffraction data acquisition at beamline 5.0.2 and Dr. Rita Nichiporuk and Dr. Anthony Iavarone (QB3/Chemistry Mass Spectrometry Facility, supported by NIH grant 1S10OD020062-01) for performing mass spectrometry. Z.J. is grateful to Dr. Alexander Schoedel, Xiang Gao, Christian Diercks, Dr. Mathieu Prevot, Dr. Roc Matheu, and Peter Waller for helpful discussions and assistance.

## ■ REFERENCES


(1) Seh, Z. W.; Kibsgaard, J.; Dickens, C. F.; Chorkendorff, I. B.; Nørskov, J. K.; Jaramillo, T. F. Combining theory and experiment in electrocatalysis: Insights into materials design. *Science* **2017**, *355*, eaad4998.

(2) McKone, J. R.; Lewis, N. S.; Gray, H. B. Will solar-driven water-splitting devices see the light of day? *Chem. Mater.* **2014**, *26*, 407−414.

(3) Clough, A. J.; Yoo, J. W.; Mecklenburg, M. H.; Marinescu, S. C. Two-dimensional metal−organic surfaces for efficient hydrogen evolution from water. *J. Am. Chem. Soc.* **2015**, *137*, 118−121.

(4) Berben, L. A.; Peters, J. C. Hydrogen evolution by cobalt tetraimine catalysts adsorbed on electrode surfaces. *Chem. Commun.* **2010**, *46*, 398−400.

(5) Xie, J.; Zhang, J.; Li, S.; Grote, F.; Zhang, X.; Zhang, H.; Wang, R.; Lei, Y.; Pan, B.; Xie, Y. Controllable disorder engineering in oxygen-incorporated $MoS_2$ ultrathin nanosheets for efficient hydrogen evolution. *J. Am. Chem. Soc.* **2013**, *135*, 17881−17888.

(6) Li, Y.; Wang, H.; Xie, L.; Liang, Y.; Hong, G.; Dai, H. $MoS_2$ nanoparticles grown on graphene: an advanced catalyst for the hydrogen evolution reaction. *J. Am. Chem. Soc.* **2011**, *133*, 7296−7299.

(7) Gao, M. R.; Chan, M. K. Y.; Sun, Y. Edge-terminated molybdenum disulfide with a 9.4-Å interlayer spacing for electrochemical hydrogen production. *Nat. Commun.* **2015**, *6*, 7493.

(8) Chen, Z.; Cummins, D.; Reinecke, B. N.; Clark, E.; Sunkara, K.; Jaramillo, T. F. Core-shelll $MoO_3$-$MoS_2$ nanowires for hydrogen evolution: a functional design for electrocatalytic materials. *Nano Lett.* **2011**, *11*, 4168−4175.

(9) Kibsgaard, J.; Jaramillo, T. F.; Besenbacher, F. Building an appropriate active-site motif into a hydrogen-evolution catalyst with thiomolybdate $[Mo_3S_{13}]^{2-}$ clusters. *Nat. Chem.* **2014**, *6*, 248−253.

(10) Merki, D.; Fierro, S.; Vrubel, H.; Hu, X. Amorphous molybdenum sulfide films as catalysts for electrochemical hydrogen production in water. *Chem. Sci.* **2011**, *2*, 1262−1267.

(11) Karunadasa, H. I.; Montalvo, E.; Sun, Y.; Majda, M.; Long, J. R.; Chang, C. J. A molecular $MoS_2$ edge site mimic for catalytic hydrogen generation. *Science* **2012**, *335*, 698−702.

(12) Jaramillo, T. F.; Jorgensen, K. P.; Bonde, J.; Nielsen, J. H.; Horch, S.; Chorkendorff, I. Identification of active edge sites for electrochemical $H_2$ evolution from $MoS_2$ nanocatalysts. *Science* **2007**, *317*, 100−102.

(13) Tran, P. D.; Tran, T. V.; Orio, M.; Torelli, S.; Truong, Q. D.; Nayuki, K.; Sasaki, Y.; Chiam, S. Y.; Yi, R.; Honma, I.; Barber, J.; Artero, V. Coordination polymer structure and revisited hydrogen




DOI: 10.1021/jacs.8b09807
J. Am. Chem. Soc. 2018, 140, 13618−13622

evolution catalytic mechanism for amorphous molybdenum sulfide. *Nat. Mater.* **2016**, *15*, 640−646.
(14) Vrubel, H.; Merki, D.; Hu, X. Hydrogen evolution catalyzed by $MoS_3$ and $MoS_2$ particles. *Energy Environ. Sci.* **2012**, *5*, 6136−6144.
(15) Kibsgaard, J.; Chen, Z.; Reinecke, B. N.; Jaramillo, T. F. Engineering the surface structure of $MoS_2$ to preferentially expose active edge sites for electrocatalysis. *Nat. Mater.* **2012**, *11*, 963−969.
(16) Wang, H.; Lu, Z.; Kong, D.; Sun, J.; Hymel, T. M.; Cui, Y. Electrochemical tuning of $MoS_2$ nanoparticles on three-dimensional substrate for efficient hydrogen evolution. *ACS Nano* **2014**, *8*, 4940−4947.
(17) Huang, Z.; Luo, W.; Ma, L.; Yu, M.; Ren, X.; He, M.; Polen, S.; Click, K.; Garrett, B.; Lu, J.; Amine, K.; Hadad, C.; Chen, W.; Asthagiri, A.; Wu, Y. Dimeric $[Mo_2S_{12}]^{2-}$ cluster: a molecular analogue of $MoS_2$ edges for superior hydrogen-evolution electrocatalysis. *Angew. Chem., Int. Ed.* **2015**, *54*, 15181−15185.
(18) Jaramillo, T. F.; Bonde, J.; Zhang, J.; Ooi, B. L.; Andersson, K.; Ulstrup, J.; Chorkendorff, I. Hydrogen evolution on supported incomplete cubane-type $[Mo_3S_4]^{4+}$ electrocatalysts. *J. Phys. Chem. C* **2008**, *112*, 17492−17498.
(19) Xie, J.; Zhang, H.; Li, S.; Wang, R.; Sun, X.; Zhou, M.; Zhou, J.; Lou, X. W.; Xie, Y. Defect-rich $MoS_2$ ultrathin nanosheets with additional active edge sites for enhanced electrocatalytic hydrogen evolution. *Adv. Mater.* **2013**, *25*, 5807−5813.
(20) Wang, H.; Lu, Z.; Xu, S.; Kong, D.; Cha, J. J.; Zheng, G.; Hsu, P. C.; Yan, K.; Bradshaw, D.; Prinz, F. B.; Cui, Y. Electrochemical tuning of vertically aligned $MoS_2$ nanofilms and its application in improving hydrogen evolution reaction. *Proc. Natl. Acad. Sci. U. S. A.* **2013**, *110*, 19701−19706.
(21) Hou, Y. D.; Abrams, B. L.; Vesborg, P. C. K.; Bjorketun, M. E.; Herbst, K.; Bech, L.; Setti, A. M.; Damsgaard, C. D.; Pedersen, T.; Hansen, O.; Rossmeisl, J.; Dahl, S.; Norskov, J. K.; Chorkendorff, I. Bioinspired molecular co-catalysts bonded to a silicon photocathode for solar hydrogen evolution. *Nat. Mater.* **2011**, *10*, 434−438.
(22) Recatala, D.; Llusar, R.; Gushchin, A. L.; Kozlova, E. A.; Laricheva, Y. A.; Abramov, P. A.; Sokolov, M. N.; Gomez, R.; Lana-Villarreal, T. Photogeneration of hydrogen from water by hybrid molybdenum sulfide clusters immobilized on titania. *ChemSusChem* **2015**, *8*, 148−157.
(23) Shang, Y. N.; Xu, X.; Wang, Z. H.; Jin, B.; Wang, R.; Ren, Z. F.; Gao, B. Y.; Yue, Q. Y. rGO/CNTs supported pyrolysis derivatives of $[Mo_3S_{13}]^{2-}$ clusters as promising electrocatalysts for enhancing hydrogen evolution performances. *ACS Sustainable Chem. Eng.* **2018**, *6*, 6920−6931.
(24) Ding, Q.; Song, B.; Xu, P.; Jin, S. Efficient electrocatalytic and photoelectrochemical hydrogen generation using $MoS_2$ and related compounds. *Chem.* **2016**, *1*, 699−726.
(25) Diercks, C. S.; Liu, Y.; Cordova, K. E.; Yaghi, O. M. The role of reticular chemistry in the design of $CO_2$ reduction catalysts. *Nat. Mater.* **2018**, *17*, 301−307.
(26) Kornienko, N.; Zhao, Y.; Kley, C. S.; Zhu, C.; Kim, D.; Lin, S.; Chang, C. J.; Yaghi, O. M.; Yang, P. Metal−organic frameworks for electrocatalytic reduction of carbon dioxide. *J. Am. Chem. Soc.* **2015**, *137*, 14129−14135.
(27) Furukawa, H.; Cordova, K. E.; O'Keeffe, M.; Yaghi, O. M. The chemistry and applications of metal−organic frameworks. *Science* **2013**, *341*, 1230444.
(28) Jiang, J.; Zhao, Y.; Yaghi, O. M. Covalent chemistry beyond molecules. *J. Am. Chem. Soc.* **2016**, *138*, 3255−3265.
(29) Wu, T.; Khazhakyan, R.; Wang, L.; Bu, X.; Zheng, S.; Chau, V.; Feng, P. Three-dimensional covalent co-assembly between inorganic supertetrahedral clusters and imidazolates. *Angew. Chem., Int. Ed.* **2011**, *50*, 2536−2539.
(30) Zheng, N.; Bu, X.; Feng, P. Self-assembly of novel dye molecules and $[Cd_8(SPh)_{12}]^{4+}$ cubic clusters into three-dimensional photoluminescent superlattice. *J. Am. Chem. Soc.* **2002**, *124*, 9688−9689.
(31) Grutza, M.; Rajagopal, A.; Streb, C.; Kurz, P. Hydrogen evolution catalysis by molybdenum sulfides ($MoS_x$): are thiomolybdate clusters like $[Mo_3S_{13}]^{2-}$ suitable active site models? *Sustainable Energy & Fuels* **2018**, *2*, 1893−1904.
(32) Muller, A.; Sarkar, S.; Bhattacharyya, R. G.; Pohl, S.; Dartmann, M. Directed synthesis of $[Mo_3S_{13}]^{2-}$, an isolated cluster containing sulfur-atoms in three different states of bonding. *Angew. Chem., Int. Ed. Engl.* **1978**, *17*, 535−536.
(33) Hegetschweiler, K.; Keller, T.; Zimmermann, H.; Schneider, W.; Schmalle, H.; Dubler, E. A new synthetic pathway for tris-$\mu$-disulfido-$\mu_3$-thio-triangulo- trimolybdenum (IV) complexes: preparation, characterization and structure of $[Mo_3S(S_2)_3(OOC\text{-}CHS\text{-}CH_2COOH)_3]^{2-}$. *Inorg. Chim. Acta* **1990**, *169*, 235−243.
(34) Llusar, R.; Uriel, S.; Vicent, C.; Clemente-Juan, J. M.; Coronado, E.; Gomez-Garcia, C. J.; Braida, B.; Canadell, E. Single-component magnetic conductors based on MO3S7 trinuclear clusters with outer dithiolate ligands. *J. Am. Chem. Soc.* **2004**, *126*, 12076−12083.
(35) Garriga, J. M.; Llusar, R.; Uriel, S.; Vicent, C.; Usher, A. J.; Lucas, N. T.; Humphrey, M. G.; Samoc, M. Synthesis and third-order nonlinear optical properties of $[Mo_3(\mu_3\text{-}S)(\mu_2\text{-}S_2)_3]^{4+}$ clusters with maleonitriledithiolate, oxalate and thiocyanate ligands. *Dalton Trans* **2003**, *23*, 4546−4551.
(36) Fedin, V. P.; Mironov, Y. V.; Virovets, A. V.; Podberezskaya, N. V.; Fedorov, V. Y. Synthesis and x-ray structure of the triangular Cluster $(Et_4N)\{[Mo_3(\mu_3\text{-}S)(\mu_2\text{-}S_2)_3(NH_2Ph)_3Br_3]Br\}Br$. *Polyhedron* **1992**, *11*, 2083−2088.
(37) Shibahara, T.; Kuroya, H. Preparation of trinuclear Molybdenum(IV) ion, $Mo_3S_4^{4+}$, and X-Ray structure of Ca-$[Mo_3S_4\{HN(CH_2CO_2)_2\}_3]\cdot 11.5H_2O$. *Polyhedron* **1986**, *5*, 357−361.
(38) Shibahara, T.; Yamasaki, M.; Sakane, G.; Minami, K.; Yabuki, T.; Ichimura, A. Syntheses and electrochemistry of incomplete cubane-type clusters with $M_3S_4$ cores (M = Mo, W). X-ray structures of $[W_3S_4(H_2O)_9](CH_3C_6H_4SO_3)_4.9H_2O$, $Na_2[W_3S_4(Hnta)_3]\cdot 5H_2O$, and $(bpyH)_5[W_3S_4(NCS)_9]\cdot 3H_2O$. *Inorg. Chem.* **1992**, *31*, 640−647.
(39) Conway, B. E.; Tilak, B. V. Interfacial processes involving electrocatalytic evolution and oxidation of $H_2$, and the role of chemisorbed H. *Electrochim. Acta* **2002**, *47*, 3571−3594.


DOI: 10.1021/jacs.8b09807
*J. Am. Chem. Soc.* 2018, 140, 13618−13622